

Chapter 6

UV Raman Spectroscopic Studies on Titania: Phase Transformation and Significance of Surface Phase in Photocatalysis

Jing Zhang, Qian Xu, Zhaochi Feng, and Can Li

Abstract Phase transformation of TiO_2 from anatase to rutile was studied by UV Raman spectroscopy with the excitation lines at 325 and 244 nm, visible Raman spectroscopy with the excitation line at 532 nm, X-ray diffraction (XRD) and transmission electron microscopy (TEM). It is found that UV Raman spectroscopy is more sensitive to the surface region of TiO_2 than visible Raman spectroscopy and XRD because TiO_2 strongly absorbs UV light. The anatase phase can be detected by UV Raman spectroscopy for the sample calcined at higher temperatures compared with that detected by visible Raman spectroscopy and XRD. It is suggested that the rutile phase nucleates at the interfaces of the contacting anatase particles; namely, for the agglomerated TiO_2 particles, the anatase phase in the inner region is easier to change into the rutile phase than that in the outer surface region. When the anatase particles are covered with highly dispersed La_2O_3 , the anatase phase can be stabilized both in the bulk and at the surface region even calcination at 900°C , owing to avoiding the direct contact of the anatase particles and occupying the surface defect sites of the anatase particles by La_2O_3 . Additionally, the La_2O_3 impregnation could effectively inhibit the growth of TiO_2 particles. The photocatalytic performance of TiO_2 samples with different surface phase structures was investigated. The surface-phase junction formed between the anatase nanoparticles and rutile particles can greatly enhance the photocatalytic activity for H_2 production.

C. Li (✉)

State Key Laboratory of Catalysis, Dalian Institute of Chemical Physics,
Chinese Academy of Sciences, Dalian, China
e-mail: canli@dicp.ac.cn

1 Instruction

Photocatalytic hydrogen production using semiconductor photocatalysts has attracted considerable interest because it has been considered an ideal method to deal with global energy problem. Among photocatalysts, TiO_2 appears to be one of the most promising and suitable materials because of its superior photocatalytic activity, chemical stability, low cost, and nontoxicity (Fujishima and Honda 1972; Grätzel 2001; Fox and Dulay 1993; Wang et al. 1997; Kamat 1993; O'Regan and Grätzel 1991). Heterogeneous photocatalysis utilizing TiO_2 materials has recently emerged as an efficient and feasible technology for the reduction of global atmospheric pollution and the purification of polluted water.

The structure of the two main polymorphs, rutile and anatase, can be discussed in terms of TiO_6 octahedrals. The two crystal structures differ by the distortion of each octahedron and by the assembly pattern of the octahedra chains (Linsebigler et al. 1995). These differences in lattice structures cause different mass densities and electronic band structures, and different physical and chemical properties. The anatase phase is suitable for catalysts and supports (Foger and Anderson 1986), while the rutile phase is used for optical and electronic purposes because of its high dielectric constant and high refractive index (Zhang et al. 1997). It has been well demonstrated that the crystalline phase of TiO_2 plays a significant role in catalytic reaction especially photocatalysis (Karakitsou and Verykios 1993; Zhu et al. 2004; Ding et al. 2000). Some studies have claimed that the anatase phase was more active than the rutile phase in photocatalysis (Karakitsou and Verykios 1993; Zhu et al. 2004).

Although at ambient pressure and temperature, the rutile phase is more thermodynamically stable than the anatase phase (Muscat et al. 2002); anatase is the common phase rather than rutile because anatase is kinetically stable in nanocrystalline TiO_2 at relatively low temperatures (Ovenston and Yanagisawa 1999). It is believed that the anatase phase transforms to the rutile phase over a wide range of temperatures (Shannon and Pask 1965). Therefore, understanding and controlling of the crystalline phase and the process of phase transformation of TiO_2 is important.

Catalytic performance of TiO_2 largely depends on the surface properties, where catalytic reaction takes place. For TiO_2 photocatalyst, the surface structure should be responsible for its photocatalytic activity because not only the photoinduced reactions take place on the surface (Linsebigler et al. 1995) but also the photoexcited electrons and holes might migrate through the surface region. Therefore, the surface phase of TiO_2 , which is exposed to the light source, should play a crucial role in photocatalysis. However, the surface phase of TiO_2 , particularly during the phase transformation has not been well investigated. The challenging question still remained: is the phase in the surface region the same as that in the bulk region, or how does the phase in the surface region of TiO_2 particle change during the bulk phase transformation? The difficulty in answering the above questions was mainly due to lacking suitable techniques that can sensitively detect the surface phase of TiO_2 .

UV Raman spectroscopy is found to be more sensitive to the surface phase of a solid sample when the sample absorbs UV light (Li et al. 2001, 2003; Li and Li 2002). This finding leads us to investigate the phase transformation in the surface region of TiO_2 by UV Raman spectroscopy as TiO_2 also strongly absorbs UV light. In this study, we compared the Raman spectra of TiO_2 calcined at different temperatures with excitation lines in the UV and visible regions. XRD and TEM were also recorded to understand the process of phase transformation of TiO_2 (Zhang et al. 2006).

2 UV Raman Spectroscopy

Raman spectroscopy is a light scattering process, which can be used to obtain information about the structure and properties of molecules from their vibrational transitions. Raman spectroscopy has been used in catalysis studies since the 1970s and it was expected that Raman spectroscopy would develop into one of the most useful techniques for the characterization of catalytic materials and catalytic reactions (Brown et al. 1977a, b; Brown and Maskovsky 1977). Although Raman spectroscopy has a number of potential applications in catalysis research, it is not as widely used in catalytic studies as expected. The main limitations are its relatively low sensitivity and

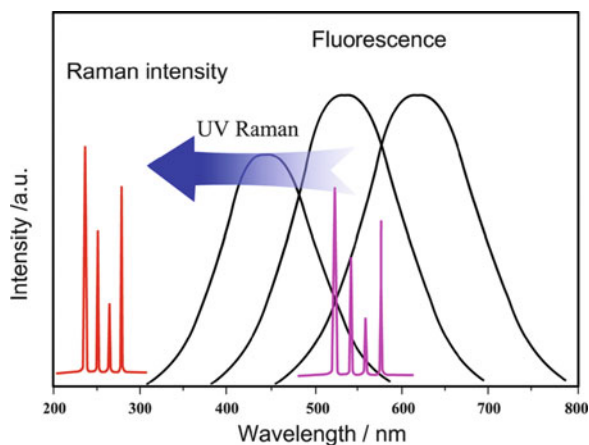


Fig. 1 The fluorescence bands appear mostly in the visible region from about 300 to 700 nm, and the Raman signal is usually obscured by the strong fluorescence interference. To avoid fluorescence interference in Raman spectrum, the Raman spectrum is shifted from the visible region to the UV region ($\lambda < 300$ nm), by shifting the excitation laser from the visible region to the UV region. Reprinted with permission from Journal of Catalysis, 216, Can Li, Identifying the isolated transition metal ions/oxides in molecular sieves and an oxide supports by UV resonance Raman spectroscopy, Copyright (2003), with permission from Elsevier

fluorescence interference (Knopps-Gerrits et al. 1997). Fluorescence interference could be avoided by shifting the excitation laser from the visible region usual for conventional Raman spectroscopy to the UV region (below 300 nm) without fluorescence interference (Fig. 1).

Since 1995, we have carried out the UV Raman spectroscopic studies of catalysts (Li and Stair 1996a) and studied sulfated zirconia (Li and Stair 1996b), coked catalysts (Li and Stair 1997; Li et al. 2000), zeolites and alumina-supported oxides (Xiong et al. 1999, 2000a, b; Li et al. 1999) and that all these have a strong fluorescence background in their visible Raman spectra, but are free of fluorescence interference in the UV Raman spectra. Hence, UV Raman spectroscopy opens up the possibility of characterizing those catalysts which are difficult to study by conventional visible Raman spectroscopy.

For UV Raman spectroscopy, not only is fluorescence avoided (Li 2003), but also the sensitivity can be improved (Stair and Li 1997). The Raman scattering intensity can be enhanced when the excitation laser is shifted from the visible (for conventional Raman) to the UV region because the Raman scattering is proportional to $1/\lambda^4$ (where λ is the wavelength of the scattering light, approximately that of the excitation laser). Furthermore, the Raman scattering can be greatly enhanced by the resonance Raman Effect, when the UV laser falls in the region of the electronic absorption of the samples.

More interestingly, UV Raman spectroscopy is found to be more sensitive to the surface phase of a solid sample when the sample absorbs UV light (Li et al. 2001, 2003; Li and Li 2002). We studied the phase transition of zirconia (ZrO_2) from tetragonal phase to monoclinic phase by UV Raman spectroscopy, visible Raman spectroscopy and XRD. Electronic absorption of ZrO_2 in the UV region makes UV Raman spectroscopy more surface sensitive than XRD or visible Raman spectroscopy. Zirconia transforms from the tetragonal phase to the monoclinic phase with calcination temperatures elevated and monoclinic phase is always detected first by UV Raman spectroscopy for the samples calcined at lower temperatures than that by XRD and visible Raman spectroscopy. UV Raman spectra clearly indicate that the surface phase of ZrO_2 is usually different from the bulk phase of ZrO_2 . Furthermore, the phase transition takes place initially at the surface regions and then gradually develops into its bulk when the ZrO_2 with tetragonal phase is calcined at elevated temperatures (Fig. 2).

For $\text{Y}_2\text{O}_3\text{-ZrO}_2$ and $\text{La}_2\text{O}_3\text{-ZrO}_2$, the transformation of the bulk phase from the tetragonal to the monoclinic is significantly retarded by the presence of yttrium oxide and lanthanum oxide (Li et al. 2003). However, the tetragonal phase in the surface region is difficult to stabilize, particularly when the content of stabilizer is low. The phase in the surface region can be more effectively stabilized by lanthanum oxide than yttrium oxide even though zirconia seemed to provide more enrichment in the surface region of the $\text{La}_2\text{O}_3\text{-ZrO}_2$ sample than the $\text{Y}_2\text{O}_3\text{-ZrO}_2$ sample, based on XPS analysis. Based on these findings, it is possible for us to further investigate the phase transformation, especially in the surface region of TiO_2 by UV Raman spectroscopy.

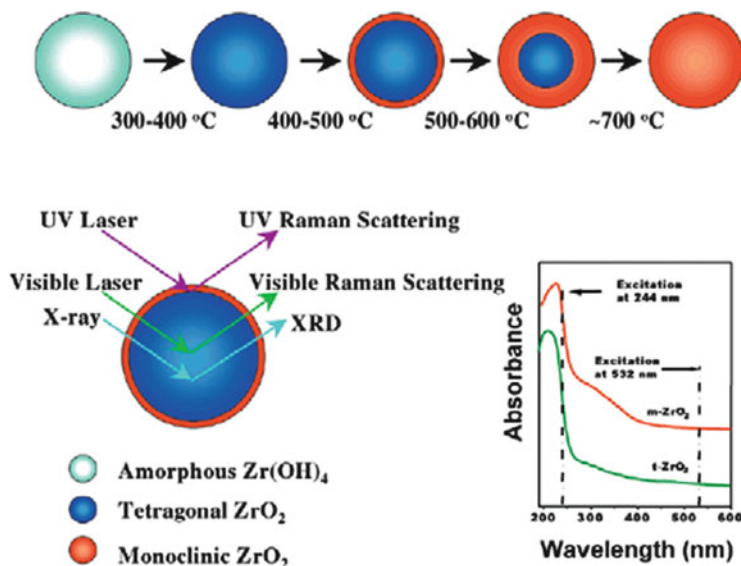


Fig. 2 Schematic description of the phase evolution of zirconia calcined at different temperatures and the information obtained from UV Raman spectroscopy, visible Raman spectroscopy, and XRD. The inset is the UV-visible absorbance of m-ZrO₂ and t-ZrO₂. Reprinted with permission from Li et al. Copyright 2001 American Chemical Society

3 Spectral Characteristics of Anatase and Rutile TiO₂

Figure 3 shows UV-Vis diffuse reflectance spectra of the TiO₂ with anatase and rutile phase, respectively. For the anatase phase, the maximum absorption and the absorption band edge can be estimated to be around 324 and 400 nm, respectively. The maximum absorption and the absorption band edge shift to a little bit longer wavelength for the rutile phase (Bickley et al. 1991).

The anatase and rutile phase of TiO₂ can be sensitively identified by Raman spectroscopy. The anatase phase shows major Raman bands at 144, 197, 399, 515, 519 (superimposed with the 515 cm⁻¹ band), and 639 cm⁻¹ (Ohsaka et al. 1978). These bands can be attributed to the six Raman-active modes of anatase phase with the symmetries of E_g, E_g, B_{1g}, A_{1g}, B_{1g}, and E_g, respectively (Ohsaka et al. 1978). The typical Raman bands due to rutile phase appear at 143 (superimposed with the 144 cm⁻¹ band due to anatase phase), 235, 447, and 612 cm⁻¹, which can be ascribed to the B_{1g}, two-phonon scattering, E_g, and A_{1g} modes of rutile phase, respectively (Chaves et al. 1974; West 1984). Additionally, the band at 144 cm⁻¹ is the strongest one for the anatase phase and the band at 143 cm⁻¹ is the weakest one for the rutile phase. Figure 4a, b display the Raman spectra of anatase and rutile TiO₂ with excitation lines at 532, 325, and 244 nm, respectively. Obviously, both visible Raman spectra and UV Raman spectra show that the TiO₂ sample is in the anatase and rutile phase.

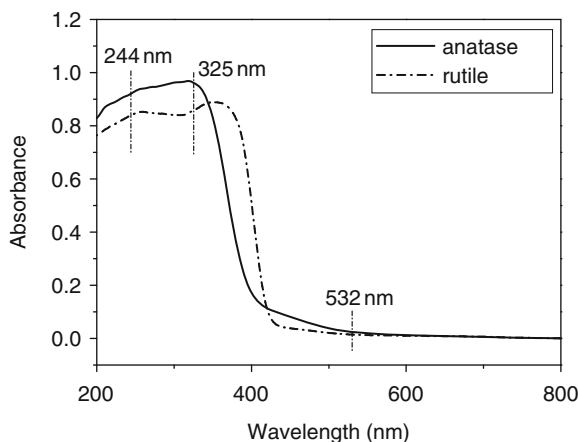


Fig. 3 UV-Vis diffuse reflectance spectra of TiO₂ calcined at 500 and 800°C. Reprinted with permission from Zhang et al. Copyright 2006. American Chemical Society

By comparing the Raman spectra of the anatase (Fig. 4a) or rutile phase (Fig. 4b) excited by 532, 325, and 244 nm lines, it is found that the relative intensities of characteristic bands due to anatase or rutile phase in the high frequency region are different. For the anatase phase (Fig. 4a), the band at 638 cm⁻¹ is the strongest one in the Raman spectrum with the excitation line at 325 or 532 nm while the band at 395 cm⁻¹ is the strongest one in the Raman spectrum with the excitation line at 244 nm.

For the rutile phase (Fig. 4b), the intensities of the bands at 445 and 612 cm⁻¹ are comparable in the visible Raman spectrum. The intensity of the band at 612 cm⁻¹ is stronger than that of the band at 445 cm⁻¹ in the Raman spectrum with the excitation line at 325 nm and the fact is reverse for the Raman spectrum with the excitation line at 244 nm. In addition, for the rutile phase, a band at approximately 826 cm⁻¹ appears in the UV Raman spectra. Some investigations show that the rutile phase of TiO₂ exhibits a weak band at 826 cm⁻¹ assigned to the B_{2g} mode (Chaves et al. 1974; West 1984).

The fact that the relative intensities of the Raman bands of anatase phase or rutile phase are different for UV Raman spectroscopy and the visible Raman spectroscopy are mainly due to the UV resonance Raman effect because the laser lines at 325 and 244 nm are in the electronic absorption region of TiO₂ (Fig. 3). There is no resonance Raman Effect observed for the TiO₂ sample excited by visible laser line because the line at 532 nm is outside of the absorption region of TiO₂ (Fig. 3). Therefore, for the anatase or rutile phase, the Raman spectroscopic characteristics in the visible Raman spectrum are different from those in the UV Raman spectrum. When different excitation lines of UV Raman spectroscopy are used, the resonance enhancement effect on the Raman bands of anatase or rutile phase is different. For example, for the rutile phase (Fig. 4b), the band at 612 cm⁻¹ is easily resonance enhanced when the excitation wavelength is 325 nm. Among all

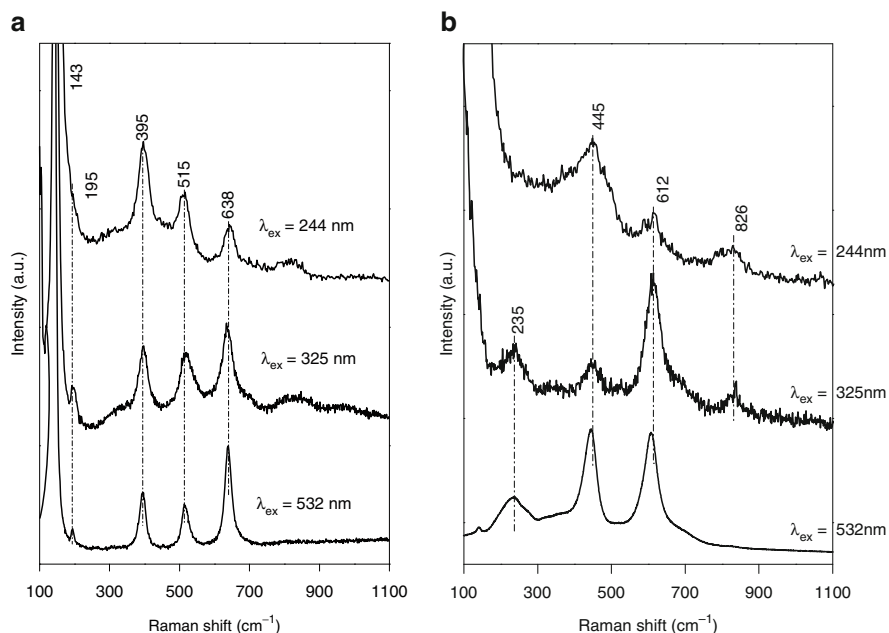


Fig. 4 (a) Raman spectra of TiO₂ calcined at 500°C with excitation lines at 532, 325, and 244 nm ($\lambda_{\text{ex}} = 532, 325, \text{ and } 244 \text{ nm}$). Reprinted with permission from Zhang et al. Copyright 2006 American Chemical Society. (b) Raman spectra of TiO₂ calcined at 800°C with excitation lines at 532, 325, and 244 nm ($\lambda_{\text{ex}} = 532, 325, \text{ and } 244 \text{ nm}$). Reprinted with permission from Zhang et al. Copyright 2006 American Chemical Society

the characteristic bands of the rutile phase, the extent of resonance enhancement of 445 cm⁻¹ is the strongest when the 244 nm laser is used as the excitation source (Fig. 4b).

4 Semiquantitative Analysis of the Phase Composition of TiO₂ by XRD and Raman Spectroscopy

The weight fraction of the rutile phase in the TiO₂ sample, W_R , can be estimated from the XRD peak intensities using the following formula (Gribb and Banfield 1997):

$$W_R = 1/[1 + 0.884(A_{\text{ana}}/A_{\text{rut}})]$$

Where A_{ana} and A_{rut} represent the X-ray integrated intensities of anatase (101) and rutile (110) diffraction peaks, respectively.

To estimate the weight fraction of the rutile phase in the TiO_2 sample by Raman spectroscopy, pure anatase phase and pure rutile phase of the TiO_2 sample, which have been prepared by calcination of TiO_2 powder at 500 and 800°C for 4 h, were mechanically mixed at given weight ratio and ground carefully to mix sufficiently.

Figure 5a displays the visible Raman spectra of the mechanical mixture with 1:1, 1:5, 1:10, 1:15, 5:1, and 10:1 ratios of anatase phase to rutile phase. The relationship between the area ratios of the visible Raman band at 395 cm^{-1} for anatase phase to the band at 445 cm^{-1} for rutile phase ($A_{395\text{cm}^{-1}}/A_{445\text{cm}^{-1}}$) and the weight ratios of anatase phase to rutile phase ($W_{\text{A}}/W_{\text{R}}$) is plotted in Fig. 5b. It can be seen that a linear relationship between the band area ratios and the weight ratios of anatase phase to rutile phase in the mixture is obtained. The rutile content in the Degussa P25, which usually consists of roughly about 80% anatase and 20% rutile phase (Yan et al. 2005) was estimated by this plot. Our Raman result indicates that the rutile content in the Degussa P25 is about 18.7%, which is close to the known result. Thus, above linear relationship based on visible Raman spectroscopy can be used to estimate the rutile content in TiO_2 .

Figure 6a presents the UV Raman spectra of mechanical mixture with 1:1, 1:2, 1:4, 1:6, 1:10, and 1:15 ratios of anatase phase to rutile phase with the excitation line at 325 nm. Figure 6b shows the plot of the area ratios of the UV Raman band at 612 cm^{-1} for rutile phase to the band at 638 cm^{-1} for anatase phase ($A_{612\text{cm}^{-1}}/A_{638\text{cm}^{-1}}$) versus the weight ratios of rutile phase to anatase phase ($W_{\text{R}}/W_{\text{A}}$). There is also a linear relationship between the band area ratios and the weight ratios of rutile phase to anatase phase.

5 Phase Transformation of TiO_2 at Elevated Calcination Temperatures

Many studies (Ovenstone and Yanagisawa 1999; Shannon and Pask 1965; Zhang and Banfield 2000a; Gouma and Mills 2001; Penn and Banfield 1999; Ma et al. 1998; Zhang et al. 1998; Busca et al. 1994; Hwu et al. 1997; Okada et al. 2001; Yoshinaka et al. 1997; Yang et al. 2000; Ozaki and Iida 1961; Navrotsky and Kleppa 1967; Ahonen et al. 1999; Lee and Zuo 2004; Ranade et al. 2002; Zhang and Banfield 2000b) have been carried out to understand the process of the phase transformation of TiO_2 . Shannon and Pask (1965) studied the phase transformation of anatase single crystals. They showed that the rutile phase nucleated at the surface and spread into the internal anatase phase during the phase transition, and the rutile phase has a slower surface energy compared to that of the anatase phase. Lee and Zuo (2004) studied the growth and phase transformation of nanometer-sized titanium oxide powders prepared by the precipitation method. In situ TEM observations showed

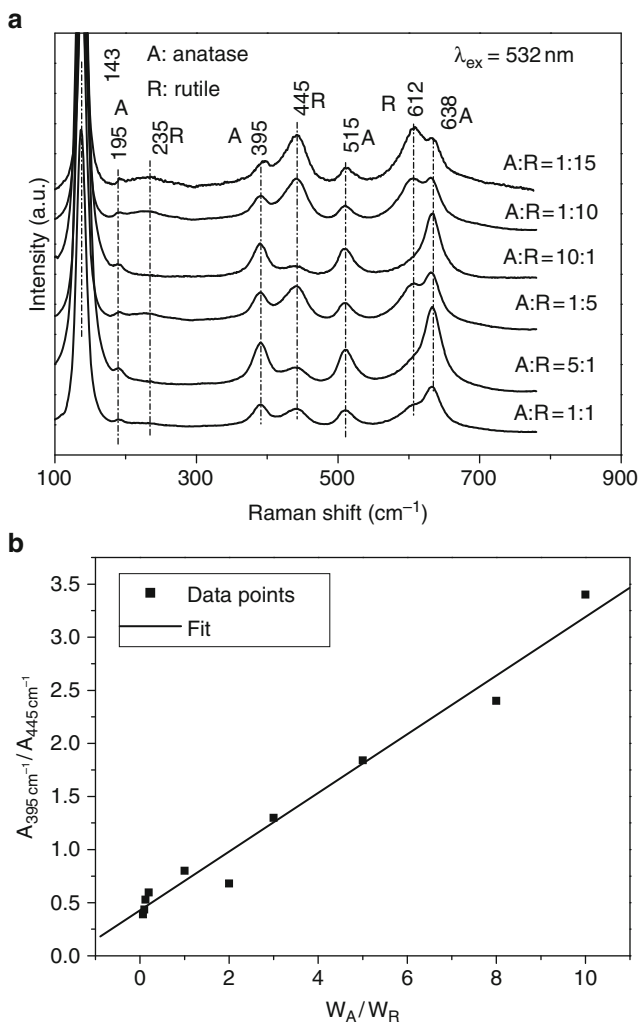


Fig. 5 (a) Visible Raman spectra of mechanical mixture with 1:1, 1:5, 1:10, 1:15, 5:1, and 10:1 ratios of anatase phase to rutile phase with the excitation line at 532 nm. (b) Plot of the area ratios of the visible Raman band at 395 cm^{-1} for anatase phase to the band at 445 cm^{-1} for rutile phase ($A_{395 \text{ cm}^{-1}}/A_{445 \text{ cm}^{-1}}$) versus the weight ratios of anatase phase to rutile phase (W_A/W_R). Reprinted with permission from Zhang et al. Copyright 2006 American Chemical Society

that the anatase particles were absorbed into rutile, and then rutile particles grew by coalescence (Fig. 7).

Zhang and Banfield (2000a) proposed that the mechanism of anatase-rutile phase transformation was temperature-dependent according to the kinetic data from XRD. The predominant nucleation mode may change from interface nucleation at low temperatures to surface nucleation at intermediate temperatures and to bulk

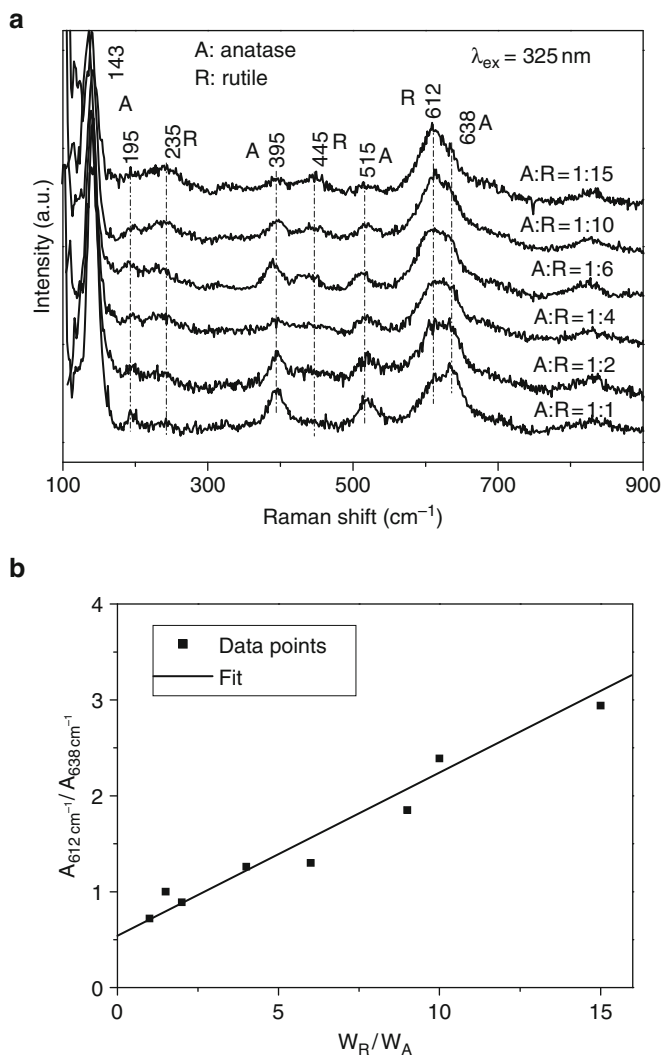


Fig. 6 (a) UV Raman spectra of mechanical mixture with 1:1, 1:2, 1:4, 1:6, 1:10, and 1:15 ratios of anatase phase to rutile phase with the excitation line at 325 nm. (b) Plot of the area ratios of the UV Raman band at 612 cm^{-1} for rutile phase to the band at 638 cm^{-1} for anatase phase ($A_{612 \text{ cm}^{-1}}/A_{638 \text{ cm}^{-1}}$) versus the weight ratios of rutile phase to anatase phase (W_R/W_A). Reprinted with permission from Zhang et al. Copyright 2006 American Chemical Society

nucleation at very high temperatures (Fig. 8). Based on transmission and scanning electron microscopy, Gouma and Mills (2001) suggested that rutile nuclei formed on the surface of coarser anatase particles and the newly transformed rutile particles grew at the expense of neighboring anatase particles. Penn and Banfield (1999)

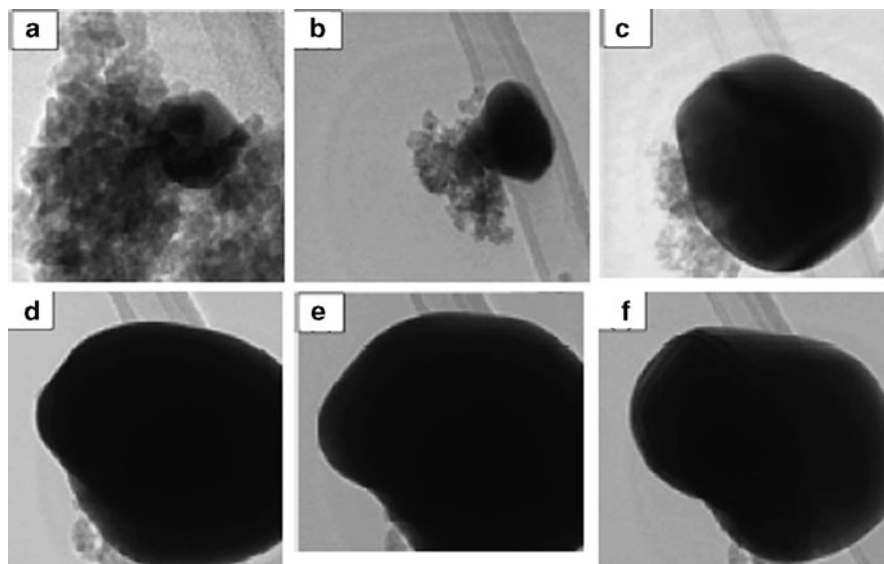


Fig. 7 In situ TEM observation of rutile particle growth. The TEM micrographs show the absorption of the anatase particles into a rutile particle heated at (a) 710° C, (b) 800° C (0 min), (c) 800° C (31 min), (d) 800° C (160 min), (e) 800° C (211 min), and (f) after cooling. Reprint with permission from Lee and Zuo. Copyright 2004 Wiley

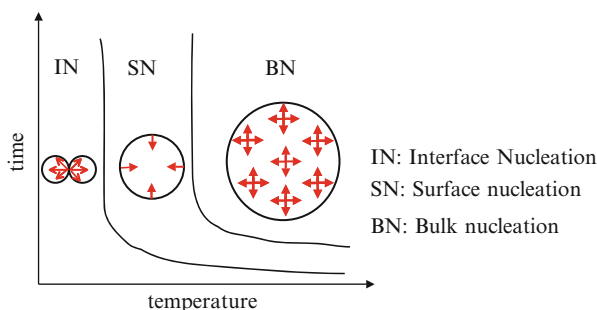


Fig. 8 The time and temperature dependence of the three dominant regions. Reprinted with permission from Zhang et al. Copyright 2000 Wiley

suggested that the formation of rutile nuclei at {112} twin interfaces of anatase particles heated hydrothermally (Fig. 9).

Figure 10 shows the XRD patterns of TiO₂ calcined at different temperatures. The “A” and “R” in the figure denote the anatase and rutile phases, respectively. For the sample before calcination, diffraction peaks due to the crystalline phase are not observed, suggesting that the sample is still in the amorphous phase. When the sample was calcined at 200°C, weak and broad peaks at $2\theta = 25.5, 37.9, 48.2, 53.8,$ and 55.0° are observed. These peaks represent the indices of (101), (004), (200), (105), and (211)

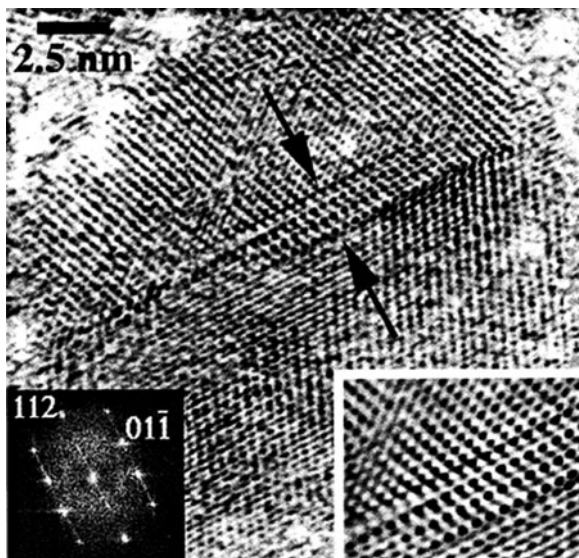


Fig. 9 Rutile nuclei (indicated *arrows*) on the {112} anatase twin surface (viewed down [131] anatase). Inset (lower right) shows rotationally filtered interface. Reproduced with permission from Penn et al. Copyright 1999 from the Mineralogical Society of America

planes of anatase phase, respectively (Sreethawong et al. 2005). These results suggest that some portions of the amorphous phase transform into the anatase phase. The diffraction peaks due to anatase phase develop with increasing the temperature of calcination. When the calcination temperature was increased to 500°C, the diffraction peaks due to anatase phase become narrow and intense in intensity. This indicates that the crystallinity of the anatase phase is further improved (Tsai and Cheng 1997).

When the sample was calcined at 550°C, weak peaks are observed at $2\theta = 27.6, 36.1, 41.2,$ and 54.3° , which correspond to the indices of (110), (101), (111), and (211) planes of rutile phase (Sreethawong et al. 2005). This indicates that the anatase phase starts to transform into the rutile phase at 550°C. The diffraction peaks of anatase phase gradually diminish in intensity and the diffraction patterns of rutile phase become predominant with the calcination temperatures from 580 to 700°C. These results clearly show that the phase transformation from anatase to rutile progressively proceeds at the elevated temperatures. The diffraction peaks assigned to anatase phase disappear at 750°C, indicating that the anatase phase completely changes into the rutile phase. The diffraction peaks of rutile phase become quite strong and sharp after the sample was calcined at 800°C, owing to the high crystallinity of the rutile phase.

Figure 11 displays the visible Raman spectra of TiO₂ calcined at different temperatures. For the sample before calcination, two broad bands at about 430 and 605 cm⁻¹ are observed, indicating that the sample is in the amorphous phase (Zhang et al. 1998). For the sample calcined at 200°C, a Raman band at 143 cm⁻¹ is observed and the high frequency region is interfered by fluorescence background,

which might come from organic species. After calcination at 300°C, other characteristic bands of anatase phase appear at 195, 395, 515, and 638 cm^{-1} , but some portions of the sample may exist in the amorphous phase because there is still broad background in Fig. 6.

It is found that, when the sample was calcined at 400°C, the fluorescence disappears possibly because the organic residues were removed by the oxidation. The bands of anatase phase increase in intensity and decrease in line width when the sample was calcined at 500°C. This result suggests that the crystallinity of the anatase phase is greatly improved (Ma et al. 1998), which is confirmed by XRD (Fig. 10). Besides the bands at 395, 515, and 638 cm^{-1} , two very weak bands at 320 and 796 cm^{-1} are observed. These two bands can be assigned to a two-phonon scattering band and a first overtone of B_{1g} at 396 cm^{-1} , respectively (Ohsaka et al. 1978). It is noteworthy that a very weak band appears at 445 cm^{-1} due to rutile phase for the sample calcined at 550°C. This indicates that the anatase phase starts to change into the rutile phase at 550°C. This result is in good agreement with that of XRD patterns (Fig. 10). The weight percentage of the rutile phase in the samples

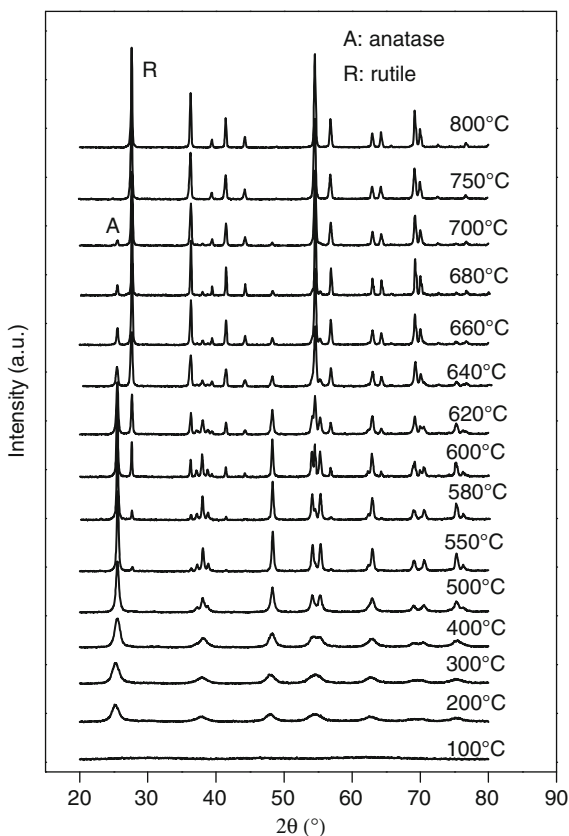
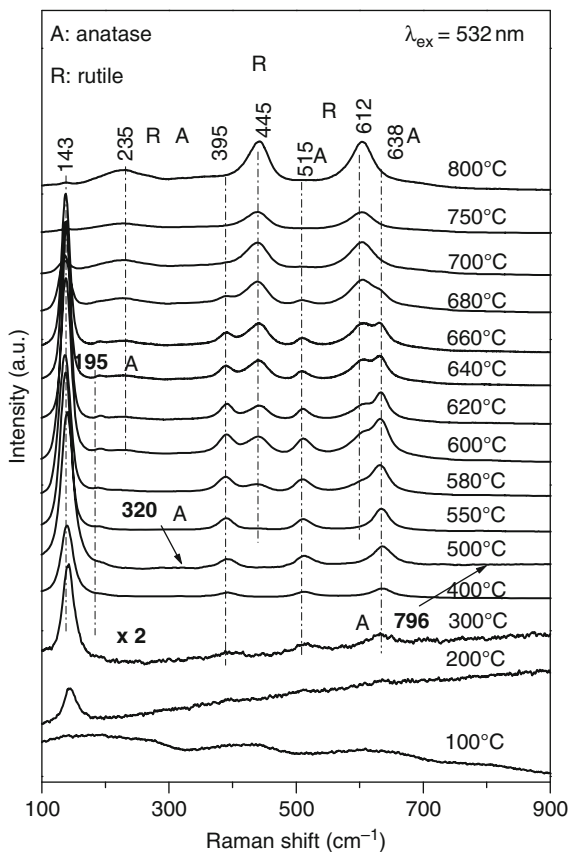


Fig. 10 XRD patterns of TiO₂ calcined at different temperatures. Reprinted with permission from Zhang et al. Copyright 2006 American Chemical Society

Fig. 11 Visible Raman spectra of TiO₂ calcined at different temperatures with the excitation line at 532 nm. Reprinted with permission from Zhang et al. Copyright 2006 American Chemical Society



calcined at different temperatures was estimated by visible Raman spectroscopy and XRD (shown in Fig. 12). As seen from Fig. 12, the rutile content estimated from visible Raman spectrum and XRD pattern of the sample calcined at 550°C is 4.2 and 5.7%, respectively. It can be seen that the rutile content estimated by visible Raman spectroscopy and XRD is also in accordance with each other.

When the sample was calcined at 580°C, the other two characteristic bands are observed at 235 and 612 cm⁻¹ due to Raman-active modes of rutile phase. Figure 12 shows that the rutile content is 13.6 and 10.9% based on the visible Raman spectrum and XRD pattern of the sample calcined at 580°C. The intensities of the bands of rutile phase (235, 445, and 612 cm⁻¹) increase steadily while those of the bands of anatase phase (195, 395, 515, and 638 cm⁻¹) decrease when the calcination temperatures were elevated from 600 to 680°C (Fig. 11). These results suggest that the TiO₂ sample undergoes the phase transformation from anatase to rutile gradually. The rutile content was estimated for the samples calcined from 600 to 680°C based on the visible Raman spectra. The result shows that the content of the rutile phase is increased from 33.1 to 91.2% respectively for the samples calcined at

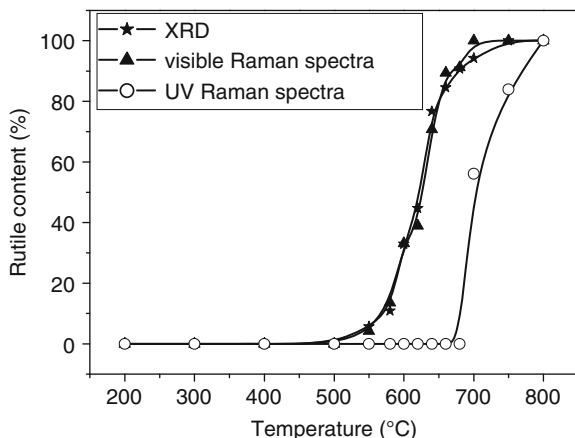


Fig. 12 The weight percentage of the rutile phase in the TiO_2 sample calcined at different temperatures estimated by visible Raman spectroscopy, XRD, and UV Raman spectroscopy

600 and 680°C (Fig. 12). The XRD results corresponding to the above two samples indicate that the rutile content is changed from 32.9 to 90.7% (Fig. 12). These results clearly show that the rutile content in the sample estimated by visible Raman spectroscopy is agreement with that estimated by XRD.

The Raman spectrum of the sample calcined at 700°C shows mainly the characteristic bands of rutile phase, but the very weak bands of anatase phase are still observed (Fig. 11). When the sample was calcined at 750°C, the bands of anatase phase disappear and only the bands due to rutile phase (143, 235, 445, and 612 cm^{-1}) are observed. These results indicate that the anatase phase completely transforms into the rutile phase, which are consistent with the results from XRD (Fig. 10). When the temperature was increased to 800°C, the intensity of characteristic bands due to rutile phase increase further.

Both the results of XRD and visible Raman spectra (Figs. 10 and 11) show that the anatase phase appears at around 200°C and perfect anatase phase is formed after calcination at temperature 400–500°C. The rutile phase starts to form at 550°C, and the anatase phase completely transforms into the rutile phase at 750°C. The signals of visible Raman spectra come mainly from the bulk region of TiO_2 because the TiO_2 sample is transparent in the visible region (Fig. 3) (Li et al. 2001, 2003; Li and Li 2002). XRD is known as a bulk sensitive technique. Therefore, it is essentially in agreement between the results of visible Raman spectra and XRD patterns.

UV-Vis diffuse reflectance spectra (Fig. 3) clearly show that TiO_2 has strong electronic absorption in the UV region. Thus, the UV Raman spectra excited by UV laser line contain more signal from the surface skin region than the bulk of the TiO_2 sample because the signal from the bulk is attenuated sharply due to the strong absorption (Li et al. 2001, 2003; Li and Li 2002). Therefore, if a UV laser line in the absorption region of TiO_2 is used as the excitation source of Raman spectroscopy, the information from UV Raman spectra is often different from that of visible Raman spectra.

The laser line at 325 nm was selected as the excitation source of the UV Raman spectra. The UV Raman spectra and the content of the rutile phase of the TiO₂ sample calcined at different temperatures are shown in Figs. 13a and 12, respectively. When the sample was calcined at 200 or 300°C, the Raman band at 143 cm⁻¹ with a shoulder band at 195 cm⁻¹ together with three broad bands at 395, 515, and 638 cm⁻¹ are observed, indicating that the anatase phase is formed in the sample. But the low intensity and the broad band indicate that the amorphous phase still remains in the sample. It can be seen that the fluorescence in the high frequency region can be avoided when the UV laser line is used as the excitation line. However, the corresponding visible Raman spectra (Fig. 11) are interfered by the fluorescence.

All bands assigned to anatase phase become sharp and strong after calcination at 500°C (Fig. 13a). These results are in agreement with those of XRD and visible Raman spectra (Figs. 10 and 11). The UV Raman spectra of the sample with the calcination temperatures from 550 to 680°C are essentially the same as those of the sample calcined at 500°C (Fig. 13a). But according to the XRD patterns and visible Raman spectra (Figs. 10 and 11), the anatase phase starts to transform into the rutile phase at only 550°C and the anatase phase gradually changes into the rutile phase in the temperature range of 550–680°C.

After calcination at 700°C, a new band at 612 cm⁻¹ and two weak bands at 235 and 445 cm⁻¹ due to rutile phase appear while the intensities of the bands of anatase phase begin to decrease (Fig. 13a). Based on the UV Raman spectrum and XRD pattern of the sample calcined at 700°C, the rutile content in the sample is 56.1 and 97.0%, respectively (Fig. 12). It is found that the rutile content estimated by UV Raman spectroscopy is far less than that estimated by XRD.

When the sample was calcined at 750°C, the intensities of the bands due to rutile phase increase, but the intensities of the bands due to anatase phase are still strong in the UV Raman spectra (Fig. 13a). UV Raman spectrum of the sample calcined at 750°C indicates that the rutile content is 84.3% (Fig. 12). However, the results of XRD and visible Raman spectrum (Figs. 10 and 11) suggest that the anatase phase totally transforms into the rutile phase after the sample was calcined at 750°C. The characteristic bands due to anatase phase disappear and the sample is in the rutile phase after calcination at 800°C (Fig. 13a). Obviously, there are distinct differences between the results from the UV Raman spectra, visible Raman spectra, and XRD patterns. It seems that the anatase phase remains at relatively higher temperatures when detected by UV Raman spectroscopy than by XRD and visible Raman spectroscopy.

Another UV laser line at 244 nm was also selected as the excitation source of UV Raman spectroscopy in order to get further insights into the phase transformation of TiO₂. The results of the UV Raman spectra of TiO₂ calcined at different temperatures with the excitation line at 244 nm are presented in Fig. 13b. When the sample was calcined at 200°C, four broad bands were observed at 143, 395, 515, and 638 cm⁻¹, which clearly indicate that the anatase phase exists in the sample. The intensities of the Raman bands due to anatase phase (143, 395, 515, and 638 cm⁻¹) become strong after calcination at 500°C. The UV Raman spectra hardly change for

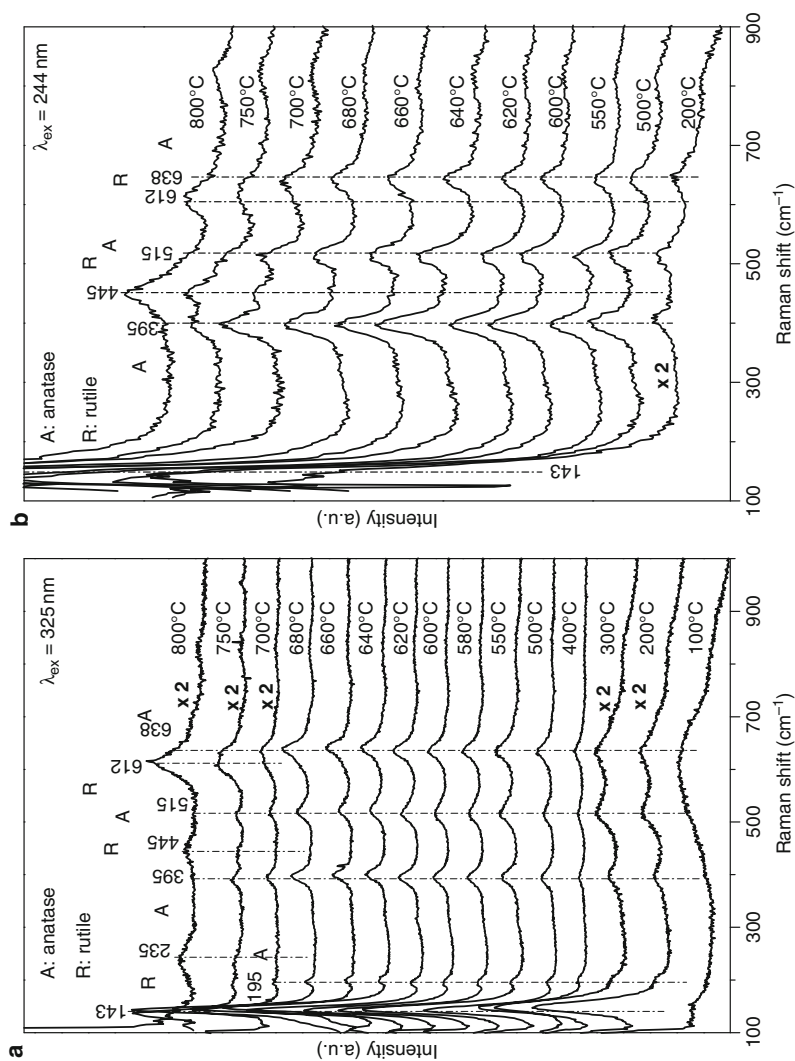


Fig. 13 (a) UV Raman spectra of TiO₂ calcined at different temperatures with the excitation line at 325 nm. Reprinted with permission from Zhang et al. Copyright 2006 American Chemical Society. (b) UV Raman spectra of TiO₂ calcined at different temperatures with the excitation line at 244 nm. Reprinted with permission from Zhang et al. Copyright 2006 American Chemical Society

the sample calcined at different temperatures even up to 680°C. The characteristic bands (445 and 612 cm^{-1}) of rutile phase appear only when the calcination temperature exceeds 700°C. This result is in good agreement with that from the UV Raman spectrum with 325 nm excitation of the sample calcined at 700°C (Fig. 13a). The intensities of the bands due to anatase phase (395, 515, and 638 cm^{-1}) decrease while those of bands assigned to rutile phase (445 and 612 cm^{-1}) increase after calcination at 750°C (Fig. 13b). When the sample was calcined at 800°C, the Raman bands due to anatase phase disappear, while the bands of rutile phase develop. This result indicates that the sample calcined at 800°C is in the rutile phase. It is interesting to note that the results of the UV Raman spectra with the excitation lines at 325 and 244 nm are consistent with each other but are different from those of XRD patterns and visible Raman spectra.

It has been clearly shown that the results of visible Raman spectra (Fig. 11) are in good agreement with the results from XRD patterns (Fig. 10) but different from those of UV Raman spectra (Fig. 13) for TiO_2 calcined at elevated temperatures. The inconsistency in the results from the three techniques can be explained by the fact that UV Raman spectroscopy provides the information mainly from surface region while visible Raman spectroscopy and XRD from bulk of TiO_2 . The discrepant results of UV Raman spectra, visible Raman spectra and XRD patterns are attributed to their different detective depth for TiO_2 particle (Li et al. 2001, 2003; Li and Li 2002).

The disagreements of UV Raman spectra, visible Raman spectra and XRD patterns suggest that the crystal phase in the surface region is different from that in the bulk during the phase transformation of TiO_2 . Busca et al. (1994) characterized the Degussa P25 using FT Raman spectroscopy and XRD technology. They estimated the rutile-to-anatase ratio by Raman spectroscopy and XRD, and found that the ratio estimated by Raman spectroscopy for the Degussa P25 was smaller than that evaluated by XRD. Therefore, they assumed that the rutile phase in the Degussa P25 was more concentrated in the bulk because Raman spectroscopy excited by near IR laser line should be more surface-sensitive than XRD. Different from their investigations, our experimental results give direct UV Raman evidences to show that the phases in the surface region are generally different from that in the bulk region of TiO_2 , particularly when TiO_2 is in the transition stage of the phase transformation.

As presented above, the anatase phase can remain at relatively higher temperatures as observed by UV Raman spectroscopy than by visible Raman spectroscopy and XRD. These facts lead us to the conclusion that the phase transformation of TiO_2 takes place from its bulk region and then extends to its surface region.

To further understand the process of the phase transformation of TiO_2 , we used TEM technique to observe the microstructure of the sample calcined at 500, 600, and 800°C (shown in Fig. 14). The most particles in the sample calcined at 500°C exhibit diameters in a range between 10 and 30 nm. On the other hand, remarkable agglomeration is observed for the TiO_2 sample calcined at 500°C. The particle size increases after calcination at 600°C. According to the results of XRD and visible Raman spectra (Figs. 10 and 11), the sample undergoes the phase transformation

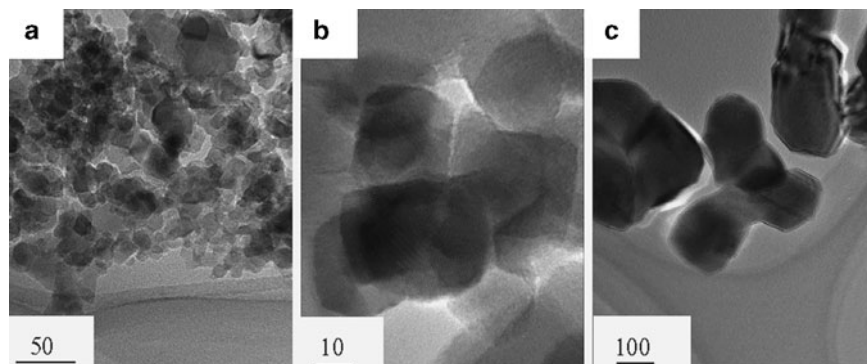


Fig. 14 TEM images of TiO_2 calcined at (a) 500°C, (b) 600°C, and (c) 800°C. Reprinted with permission from Zhang et al. Copyright 2006 American Chemical Society

from anatase to rutile gradually in the temperature range of 550–680°C. These results imply that the phase transformation and growth of the particle size are interrelated. Many researchers (Kumar 1995; Hague and Mayo 1993; Banfield et al. 1993; Mackenzie 1975; Kumar et al. 1992) reported similar phenomena. Kumar et al. (Kumar 1995) attributed this particle size growing to the higher atomic mobility because of bond breakage during the phase transformation. When the calcination temperature was increased to 800°C, TiO_2 particles further grow and the particle size can be as big as about 200 nm.

According to TEM measurements Penn and Banfield (1999) suggested that structural elements with rutilelike character can be produced at a subset of anatase interfaces, and these might serve as rutile nucleation sites. Lee and Zuo (2004) investigated the growth and transformation in nanometer-sized TiO_2 powders by in situ TEM. The nucleation of rutile was found to occur at the amorphous interface of anatase particles where there are strain and disorder. Based on the experimental observations and combined with the results from the literature, we suggest that the phase transformation of TiO_2 starts from the interfaces among the anatase particles of the agglomerated TiO_2 particles. Based on kinetic data from XRD, Zhang and Banfield (2000a) also proposed that interface nucleation dominated the transformation for nanocrystalline anatase samples with denser particle packing below 620°C, or in the temperature range of 620–680°C.

A proposed scheme for the phase transformation of TiO_2 with increasing calcination temperature is illustrated in Fig. 15. The TiO_2 particles with anatase phase intimately contact with each other. Thus, the surface and the bulk region of the TiO_2 sample actually refer to respectively the outer surface region and the inner region of agglomerated TiO_2 particles. The interfaces of contacting anatase particles, which only present in the inner region of agglomerated particles, provide the nucleation sites of the rutile phase. Therefore, the rutile phase is first detected by XRD and visible Raman spectroscopy for the sample calcined at 550–680°C. Once phase transformation takes place, the particle size increases rapidly. The agglomeration of the TiO_2 particles is along with the phase transformation from anatase to rutile.

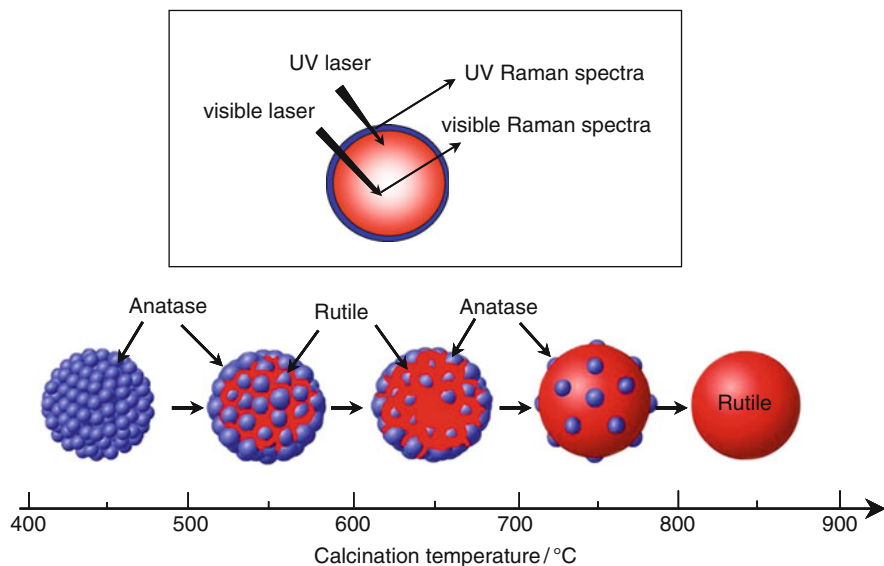


Fig. 15 A proposed scheme for the phase transformation of TiO_2 with increasing calcination temperature. Reprinted with permission from Zhang et al. Copyright 2006 American Chemical Society

The rutile phase needs fairly high temperature to progressively develop into the whole conglomeration composed of some neighboring particles coalescence as the phase transformation is a diffusing process. Thus, the outer surface region of the agglomerated particles without directly interacting with other particles maintains in the anatase phase when the calcination temperature is below 680°C . Accordingly, UV Raman spectroscopy detect only the anatase phase in the outer region of agglomerated particles in the temperature range of $550\text{--}680^\circ\text{C}$.

When the calcination temperature is higher than 700°C , the anatase phase of the outer surface region of agglomerated particles begins to change into the rutile phase. Therefore, the mixed phases of anatase and rutile are observed by UV Raman spectroscopy but the inner region of agglomerated particles is nearly in the rutile phase. Both XRD and visible Raman spectra show that the inner region of agglomerated particles is in the rutile phase when the sample is calcined at 750°C . However, the phase transformation is still not yet complete because the outer surface region is still in the mixed phases of anatase and rutile. After calcination at 800°C , the anatase phase in the outer surface region completely transforms to the rutile phase, the whole agglomerated particles are in the rutile phase.

Following the above reasoning, for the agglomerated particles of TiO_2 , the rutile phase nucleates at the interfaces of contacting anatase particles. However, from the point view of a single anatase crystal particle, the rutile phase starts to form at the surface of TiO_2 , where it is in contact with other particles. It is reasonably assumed that the phase transformation of single particle might start from the surface, where

there is no direct interaction with other particles, but it needs high temperature. Zhang et al. (Zhang and Banfield 2000a) indicated that thermal fluctuation of Ti and O atoms in anatase is not strong enough to generate rutile nuclei on the surfaces or in the bulk of the anatase particles at lower temperatures.

When the small anatase particles agglomerated into large particles, interface nucleation is easier, as compared to nucleation at the surface, where there is no contact with other particles. Zhang and Banfield (2000a) indicated that the activation energy for surfaces nucleation is expected to be higher than that for interfaces nucleation. Therefore, we observed the phenomenon that crystalline phase in the outer surface region of agglomerated TiO₂ particles is different from that in the inner region of agglomerated TiO₂ particles.

6 Phase Transformation of TiO₂ with La₂O₃ Loading

If the direct contact between anatase particles of TiO₂ is avoided, the phase transformation of TiO₂ from anatase to rutile could be retarded or prohibited. This assumption may be verified by covering the surface of anatase TiO₂ with an additive. It has been reported that La³⁺ did not enter into the crystal lattices of TiO₂ and was uniformly dispersed onto TiO₂ as the form of lanthana (La₂O₃) particles with small size (Jing et al. 2004; Xie and Tang 1990; Gopalan and Lin 1995). In order to verify the above assumption, this study also prepared the anatase phase of TiO₂ sample covered with La₂O₃ and characterized the above sample by XRD, visible Raman spectroscopy and UV Raman spectroscopy.

Figure 16a displays the visible Raman spectra of La₂O₃/TiO₂ with increasing La₂O₃ loading. TiO₂ support is in the anatase phase because only characteristic bands (143, 195, 395, 515, and 638 cm⁻¹) due to anatase phase are observed. When the TiO₂ support was calcined at 900°C (TiO₂-900), the Raman spectrum gives the characteristic bands of rutile phase, indicating that the TiO₂-900 sample is in the rutile phase. We firstly studied the crystalline phase of 6 wt% La₂O₃/TiO₂ calcined at 900°C. Only characteristic bands of anatase phase are observed, suggesting that the TiO₂ sample retains its anatase phase when La₂O₃ loading is 6 wt% while the TiO₂-900 sample is in the rutile phase. With decreasing the La₂O₃ loading to 3 or 1 wt%, it is observed that the TiO₂ sample can still be stabilized at its anatase phase.

It should be noted that TiO₂ sample maintain the anatase phase even when the La₂O₃ loading is only 0.5 wt%. The spectra of the sample with the La₂O₃ loadings from 1 to 6 wt% are almost the same as those for the sample with 0.5 wt% La₂O₃ loading, except for a small decrease in intensity. Figure 16b shows XRD patterns of La₂O₃/TiO₂ with increasing La₂O₃ loading. When the loading of La₂O₃ is varied from 0.5 to 6 wt%, it is obvious that the samples are stabilized at their anatase phase both in bulk and in the surface region even after the calcination at 900°C. The results from XRD patterns agree well with those of visible Raman spectra.

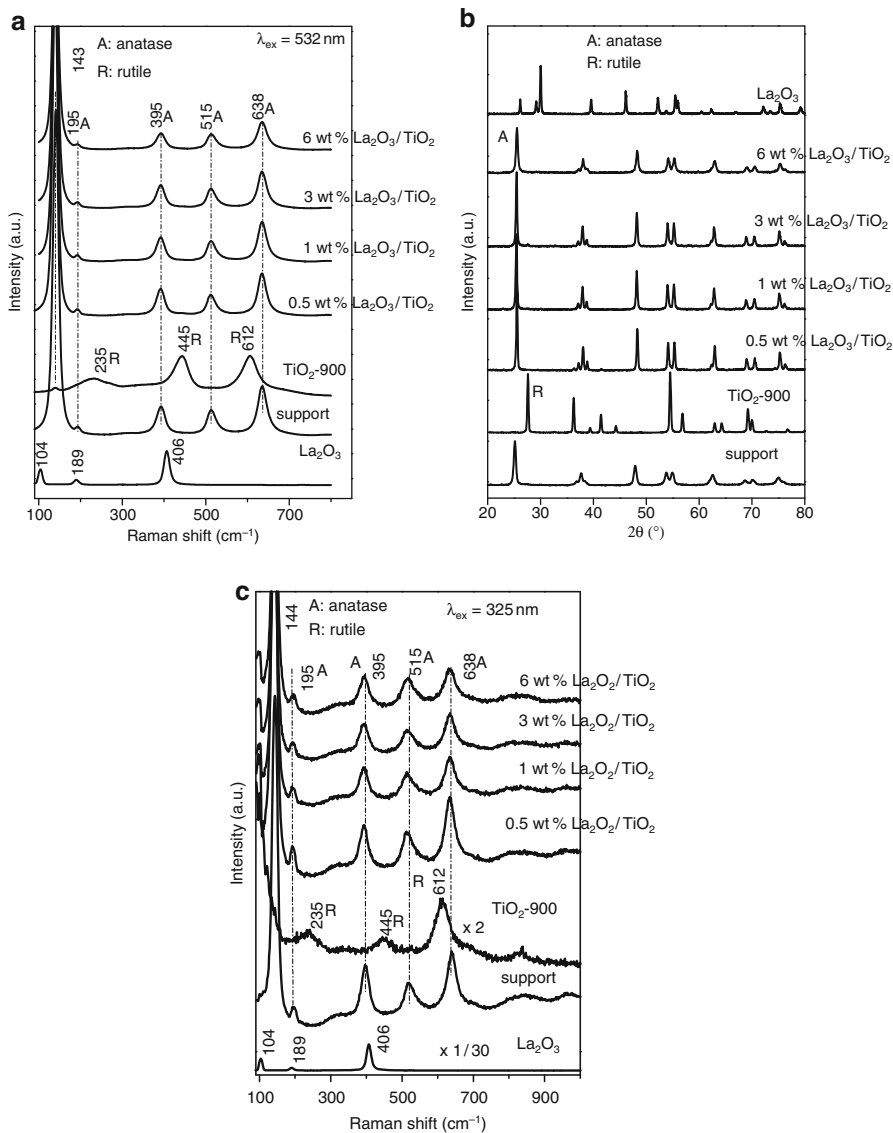


Fig. 16 (a) Visible Raman spectra, (b) XRD patterns, (c) UV Raman spectra of $\text{La}_2\text{O}_3/\text{TiO}_2$ with increasing La_2O_3 loading. Reprinted with permission from Zhang et al. Copyright 2006 American Chemical Society

Figure 16c shows the UV Raman spectra of $\text{La}_2\text{O}_3/\text{TiO}_2$ with increasing La_2O_3 loading. The Raman spectrum of the TiO_2 support and the TiO_2 -900 sample gives the characteristic bands of anatase phase and rutile phase, respectively. When La_2O_3 loading is varied from 0.5 to 6 wt%, the results of the UV Raman spectra

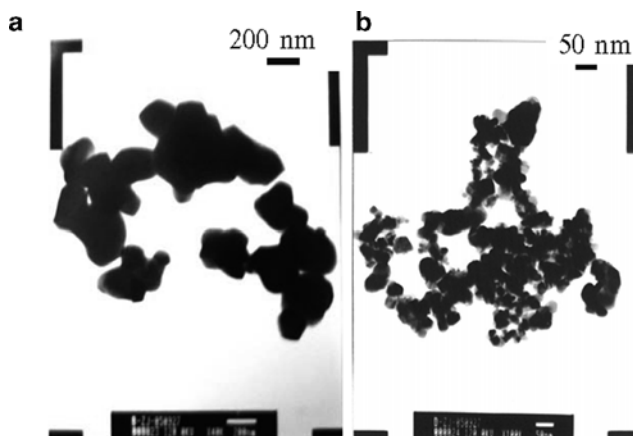


Fig. 17 TEM micrographs of (a) TiO_2 -900 and (b) 1 wt% $\text{La}_2\text{O}_3/\text{TiO}_2$ sample calcined at 900°C

show that all the samples are in the anatase phase. These results are in accordance with those of visible Raman spectra and XRD (Fig. 16a, b). For both visible Raman spectra and UV Raman spectra, no bands due to crystalline phase of La_2O_3 are observed for all the $\text{La}_2\text{O}_3/\text{TiO}_2$ samples, showing that La_2O_3 is highly dispersed on the surface of anatase phase of TiO_2 particles (Xie and Tang 1990).

Figure 17 compares the TEM micrographs of TiO_2 -900 and 1 wt% $\text{La}_2\text{O}_3/\text{TiO}_2$ sample calcined at 900°C . It could be found that the particle size is obviously decreased by addition of 1 wt% La_2O_3 . It should be noted that both TiO_2 support and 1 wt% $\text{La}_2\text{O}_3/\text{TiO}_2$ sample appear similar average particle size, demonstrating that La^{3+} impregnation could effectively inhibit the increase of TiO_2 particle size.

Combined results of XRD, visible Raman spectra and UV Raman spectra of the $\text{La}_2\text{O}_3/\text{TiO}_2$ samples (Fig. 16), showed that 0.5 wt% La_2O_3 can stabilize the anatase phase both in bulk and in the surface region even after the calcination at 900°C . We further decreased the loading of La_2O_3 and recorded the corresponding XRD patterns and UV Raman spectra. Figure 18a displays XRD patterns of $\text{La}_2\text{O}_3/\text{TiO}_2$ with La_2O_3 loading from 0.1 to 0.4 wt%. Weak peaks due to anatase phase are observed for the 0.1 wt% $\text{La}_2\text{O}_3/\text{TiO}_2$ sample in addition to the characteristic peaks attributed to the rutile phase. The XRD result corresponding to the above sample indicates that the rutile content is 95%. With increasing the loading of La_2O_3 , the diffraction peaks of rutile phase gradually diminish in intensity and the diffraction patterns of anatase phase become predominant. The result from XRD shows that the content of the rutile phase is decreased from 83 to 43% when La_2O_3 loading is increased from 0.2 to 0.4 wt%. This is strong evidence that the anatase phase of TiO_2 in the bulk can be stabilized by adding La_2O_3 . Furthermore, the bulk region retain the anatase phase only when the loading of La_2O_3 is up to 0.5 wt%.

From UV Raman spectra (Fig. 18b), some weak peaks of the rutile phase are observed, while the main pattern is due to the anatase phase when the La_2O_3 loading

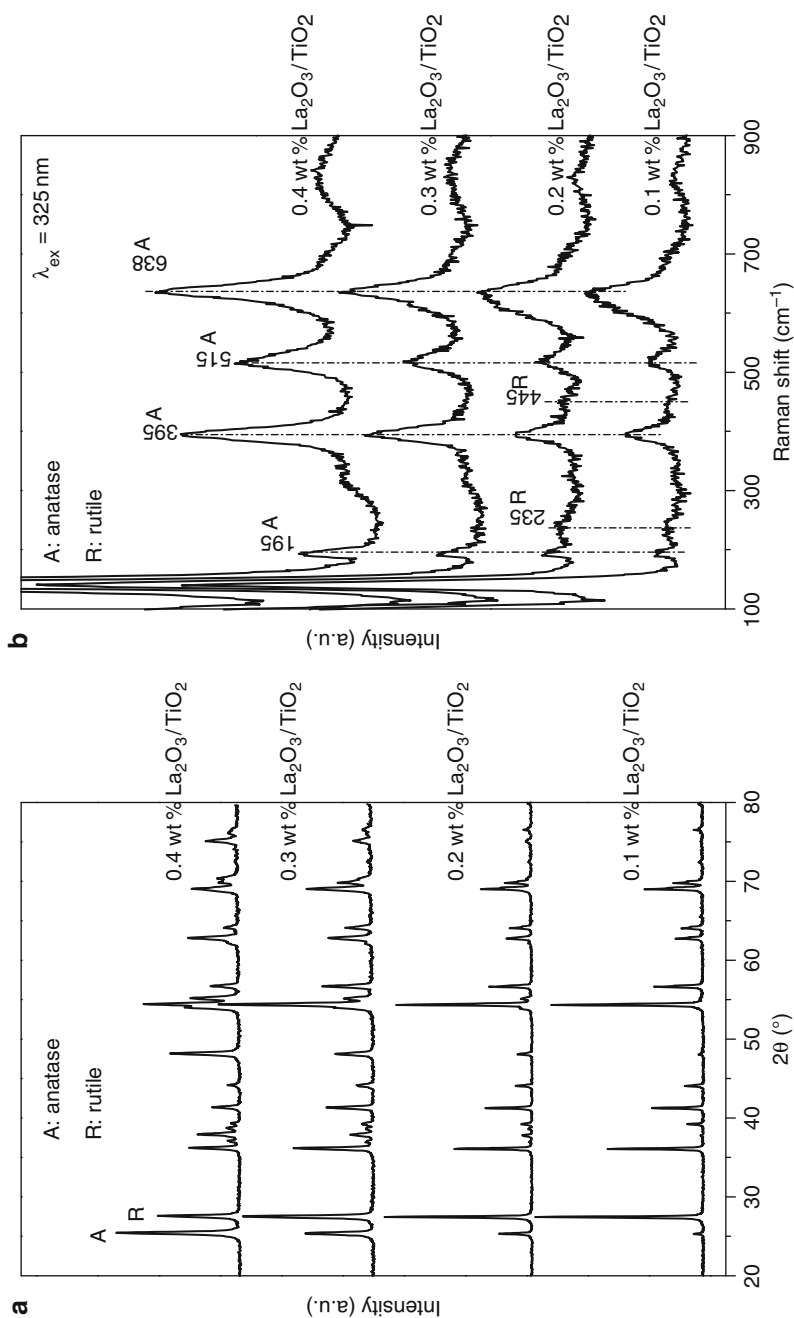


Fig. 18 (a) XRD patterns, (b) UV Raman spectra of $\text{La}_2\text{O}_3/\text{TiO}_2$ with La_2O_3 loading from 0.1 to 0.4 wt%

is 0.1 or 0.2 wt%. Further increasing the loading of La_2O_3 to 0.3 or 0.4 wt%, the surface region is stabilized at the anatase phase. Combined with the results from XRD, it can be seen that the impregnation of La_2O_3 not only stabilizes the anatase phase in the bulk region, but also retards the development of the rutile phase into the surface.

It is interesting to note that the impregnation of only 0.5 wt% La_2O_3 (3% the monolayer dispersion capacity La_2O_3 of the weight of TiO_2) can inhibit the phase transformation. The explanation of this interesting result could be as follows: the defect sites on the surface of the anatase particles are assumed to play an important role in the phase transformation of TiO_2 . When the defect sites of the anatase particle react with a neighboring anatase particle with or without defect sites, the rutile phase formation may start at these sites. La_2O_3 easily reacts with the defect sites of the anatase particles and the only 0.5 wt% La_2O_3 can occupy or deactivate all the defect sites of the anatase particles because usually the surface defect sites concentration is relatively low. The easy migration of surface atoms of anatase and the nucleation of rutile phase may most possibly take place at the surface defect sites. Therefore, only 0.5 wt% La_2O_3 can effectively inhibit the phase transformation of anatase and growing of the particle size.

In addition to occupying the defective sites, the highly dispersed La_2O_3 on the surface of the anatase particles effectively avoids the direct contact of the anatase particles for the sample with high La_2O_3 loadings. Therefore, the $\text{La}_2\text{O}_3/\text{TiO}_2$ sample can retain its anatase phase even when the calcination temperature is up to 900°C , owing to the above two roles played by La_2O_3 .

7 Photocatalytic Performance of TiO_2 with Different Surface Phase Structures

The surface phase of TiO_2 , which is directly exposed to light and the reactants, contribute to photocatalysis and solar energy conversion because the photocatalytic reaction or photoelectron conversion takes place only when photo-induced electrons and holes are available on the surface (Linsebigler et al. 1995; Sakthivel et al. 2006). The crystalline phase of TiO_2 particles in the surface region may be different from that in the bulk region (Busca et al. 1985, 1994; Zhang et al. 2006), particularly when TiO_2 is in its transition stage of the phase transformation from anatase to rutile (Zhang et al. 2006, 2008).

The rutile content in the bulk region and the anatase content in the surface region, estimated from visible and UV Raman spectra, are shown respectively by the solid curve and broken curve in Fig. 19a. The rate of H_2 evolution does not evidently change for the TiO_2 calcined from 500 to 680°C , although the amount of the rutile phase in the bulk region is greatly increased (Fig. 19b). It is obvious that the overall photocatalytic activity is more directly related to its surface phase because the anatase phase always exists in the surface region for

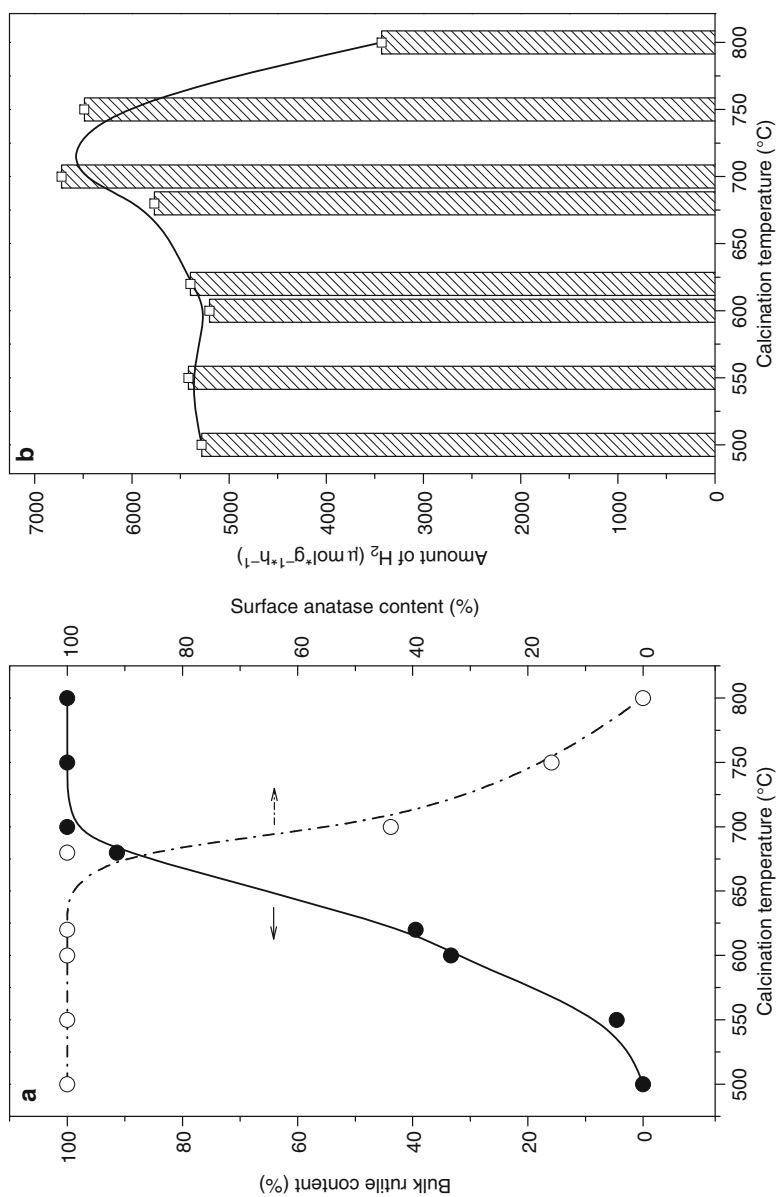


Fig. 19 (a) Dependence of bulk rutile content (filled circles, solid line) and surface anatase content (open circle, broken line), (b) TiO₂ samples calcined at different temperatures and their corresponding overall photocatalytic activity. Reprinted with permission from Zhang et al. Copyright 2008 Wiley

the samples calcined at 500–680°C. A maximum activity is observed for TiO₂ samples calcined at 700–750°C, where the bulk of TiO₂ is almost in pure rutile while the surface is in a mixed phase of anatase and rutile. The anatase phase in the surface region of TiO₂ sample is completely transformed into the rutile phase when the calcination temperature is increased to 800°C, and correspondingly the overall photocatalytic activity decreases dramatically. Thus, the pure rutile phase shows low overall activity for the H₂ production. This result suggests that the presence of the surface anatase on rutile TiO₂ can keep a relatively high overall photocatalytic activity. This effect should be attributed to the formation of surface-phase junction.

To further demonstrate if higher photocatalytic activity can be achieved for TiO₂ photocatalyst with surface junction formed between anatase and rutile TiO₂, anatase were deposited on rutile by a wet impregnation method (Loddo et al. 1999), and then the TiO₂ powder was calcined up to 400°C. To obtain the samples with different amounts of anatase on the surface of rutile, the impregnation procedure was repeated (the loading of anatase deposited on the surface of the rutile particles was roughly 5 wt% for each time). The as-prepared samples were denoted as TiO₂(A)/TiO₂(R)-n, in which TiO₂(A) indicates the surface anatase, TiO₂(R) indicates the rutile as the support, and the number n indicates the number of impregnation.

Figure 20a–c shows the SEM of TiO₂(A)/TiO₂(R)-0, 1, 4 samples, where it is clearly observed that fine anatase particles (particle size <30 nm) are highly deposited on the rutile particles (particle size ~500 nm) in the TiO₂(A)/TiO₂(R)-n samples.

The surface specific activity of TiO₂(A)/TiO₂(R) catalysts with increasing the amount of anatase on the surface of rutile are given in Fig. 20d. The anatase content estimated from XRD and UV Raman spectroscopy is also displayed in Fig. 20d. Compared with the pure rutile support, the photocatalytic activity is remarkably increased by supporting a small amount of anatase on the surface of rutile. For example, TiO₂(A)/TiO₂(R)-1,2 samples exhibit much higher photocatalytic activities despite their low surface anatase contents (<10 wt%), for TiO₂(A)/TiO₂(R)-3, the photocatalytic activity is greatly enhanced to about four times higher than that of pure rutile. This enormous increase in the photocatalytic activity can be attributed to the formation of the surface anatase/rutile phase junction. For TiO₂(A)/TiO₂(R)-4 sample, the photocatalytic activity is decreased somewhat because the surface of the rutile may be fully covered by the anatase, that decreases the amount of exposed anatase/rutile phase junction on the TiO₂ surface.

In order to visualize the surface phase junction, the TiO₂(A)/TiO₂(R)-n ($n = 1-4$) samples were investigated by HRTEM. Figure 21 shows the HRTEM result of a TiO₂(A)/TiO₂(R)-n sample. The result clearly shows that the junction structure between anatase and rutile phase is formed on the TiO₂(A)/TiO₂(R)-n sample. HRTEM gives the direct evidence for the surface anatase/rutile junction formed on rutile particles.

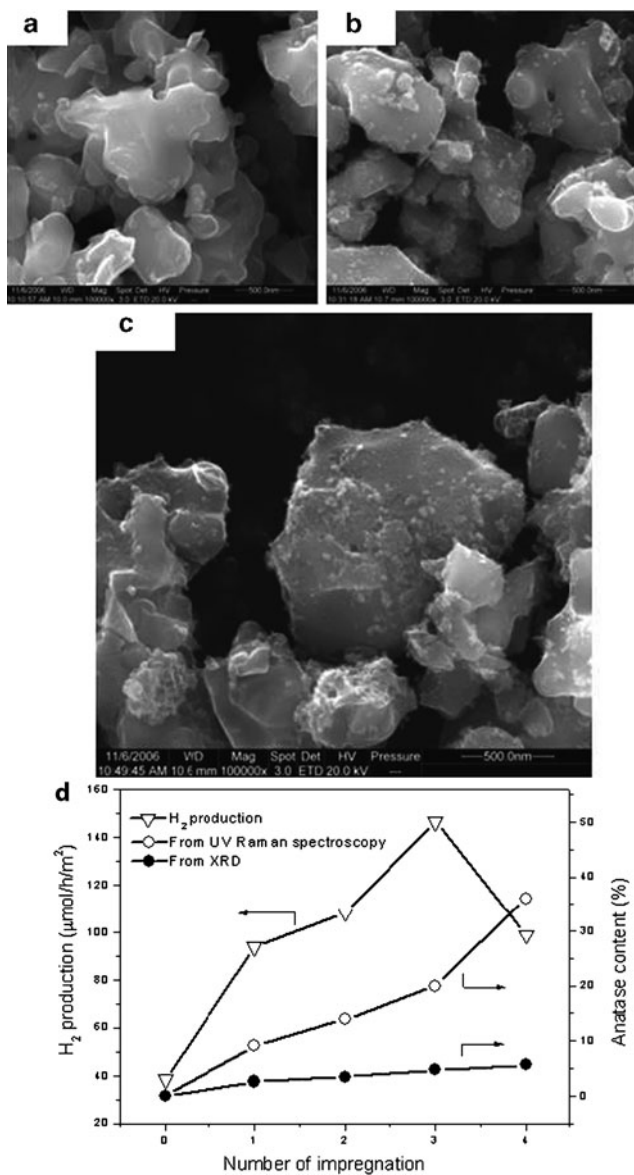


Fig. 20 Scanning electron micrographs of (a) TiO₂(R), (b) TiO₂(A)/TiO₂(R)-1, and (c) TiO₂(A)/TiO₂(R)-4 samples. (d) The photocatalytic activities for H₂ evolved per surface area of TiO₂(A)/TiO₂(R)-n samples with increasing the amount of anatase phase on the surface of rutile TiO₂. The rate of H₂ evolved per surface area of TiO₂(R) before depositing anatase TiO₂ is added for comparison. The anatase contents estimated from XRD and UV Raman spectroscopy for TiO₂(A)/TiO₂(R)-n samples are also displayed. Reprinted with permission from Zhang et al. Copyright 2008 Wiley

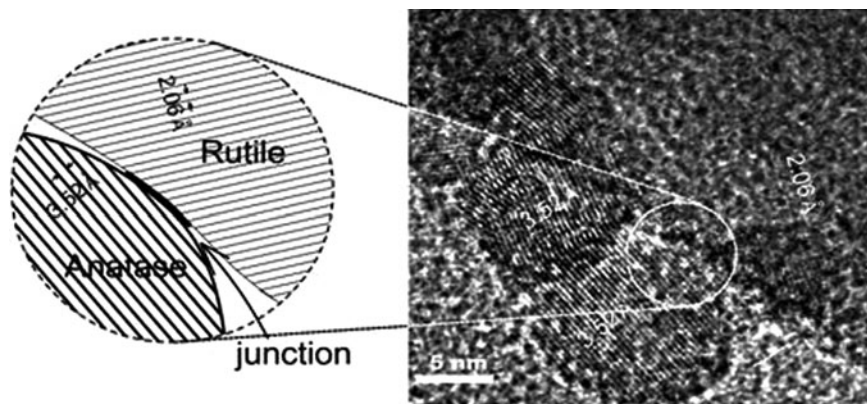


Fig. 21 HRTEM image of $\text{TiO}_2(\text{A})/\text{TiO}_2(\text{R})\text{-n}$ sample. Reprinted with permission from Zhang et al. Copyright 2008 Wiley

8 Conclusions

This chapter discussed the applications of UV Raman spectroscopy in the studies of TiO_2 , including phase transformation and significance of surface phase in photocatalysis. UV Raman spectroscopy combined visible Raman spectroscopy, XRD, and TEM indicated that the crystalline phases of TiO_2 particles in the surface region is different from that in the bulk region, particularly when TiO_2 is in its transition stage of the phase transformation from anatase to rutile.

A direct correlation between the surface phases of TiO_2 and its catalytic, especially photocatalytic performance is of great significance because catalytic reaction takes place on the surface. A great deal of research has been conducted to investigate the effect of the surface properties on the photoactivity of TiO_2 . However, the direct relationship between the photocatalytic performance and the surface phase of TiO_2 remained a challenging subject. This may be due to the difficulty to characterize the surface phase of TiO_2 , especially of TiO_2 nanoparticle, which has been practically used as a catalyst or a photocatalyst. Taking the advantage of UV Raman spectroscopy for understanding the surface phase of TiO_2 , if the photocatalytic activity of TiO_2 with different crystalline phase compositions was evaluated, it is possible to correlate the surface phase of TiO_2 and its photoactivity.

Acknowledgements This work was financially supported by the National Natural Science Foundation of China (NSFC, Grant No. 20673112), National Basic Research Program of China (Grant No. 2009CB220010), and Program for Strategic Scientific Alliances between China and the Netherlands (2008DFB50130).

References

- Ahonen PP, Kauppinen EI, Joubert JC, Deschanvres JL, Van Tendeloo G (1999) Preparation of nanocrystalline titania powder via aerosol pyrolysis of titanium tetrabutoxide. *J Mater Res* 14:3938–3948
- Banfield JF, Bischoff BL, Anderson MA (1993) TiO₂ accessory minerals: coarsening, and transformation kinetics in pure and doped synthetic nanocrystalline materials. *Chem Geol* 110:211–231
- Bickley RI, Gonzalez-Carreno T, Lees JS, Palmisano L, Tilley RJD (1991) A structural investigation of titanium dioxide photocatalysts. *J Solid State Chem* 92:178–190
- Brown FR, Maskovsky LE (1977) Raman spectra of a cobalt oxide-molybdenum oxide supported catalyst. *Appl Spectrosc* 31:44–46
- Brown FR, Maskovsky LE, Rhee KH (1977a) Raman spectra of supported molybdena catalysts. I. Oxide catalysts. *J Catal* 50:162–171
- Brown FR, Maskovsky LE, Rhee KH (1977b) Raman spectra of supported molybdena catalysts: II. sulfided, used, and regenerated catalysts. *J Catal* 50:385–389
- Busca G, Saussey H, Saur O, Lavalley JC, Lorenzelli V (1985) FT-IR characterization of the surface acidity of different titanium dioxide anatase preparations. *Appl Catal* 14:245–260
- Busca G, Ramis G, Amores JMG, Escribano VS, Piaggio P (1994) FT Raman and FT-IR studies of titanias and metatitanate powders. *J Chem Soc Faraday Trans* 90:3181–3190
- Chaves A, Katiyan KS, Porto SPS (1974) Coupled modes with asymmetry in tetragonal BaTiO₃. *Phys Rev B* 10:3522–3533
- Ding Z, Liu GQ, Greenfield PF (2000) Role of the crystallite phase of TiO₂ in heterogeneous photocatalysis for phenol oxidation in water. *J Phys Chem B* 104:4815–4820
- Foger K, Anderson JR (1986) Thermally stable SMSI supports: iridium supported on TiO₂-Al₂O₃ and on Ce-doped anatase. *Appl Catal* 23:139–155
- Fox MA, Dulay MT (1993) Heterogeneous photocatalysis. *Chem Rev* 93:341–357
- Fujishima A, Honda K (1972) Electrochemical photolysis of water at a semiconductor electrode. *Nature* 238:37–38
- Gopalan R, Lin YS (1995) Evolution of pore and phase structure of sol-gel derived lanthana doped titania at high temperatures. *Ind Eng Chem Res* 34:1189–1195
- Gouma PI, Mills MJ (2001) Anatase to rutile transformation in titania powders. *J Am Ceram Soc* 84:619–622
- Grätzel M (2001) Photoelectrochemical cells. *Nature* 414:338–344
- Gribb AA, Banfield JF (1997) Particle size effects on transformation kinetics and phase stability in nanocrystalline TiO₂. *Am Mineral* 82:717–728
- Hague DC, Mayo M (1993) Effect of crystallization and phase transformation in nanocrystalline TiO₂. *Nanostruct Mater* 3:61–67
- Hwu Y, Yao YD, Cheng NF, Tung CY, Lin HM (1997) X-ray absorption of nanocrystal TiO₂. *Nanostruct Mater* 9:355–358
- Jing LQ, Sun XJ, Xin BF, Wang BQ, Cai WM, Fu HG (2004) The preparation and characterization of La doped TiO₂ nanoparticles and their photocatalytic activity. *J Solid State Chem* 177:3375–3382
- Kamat PV (1993) Photochemistry on nonreactive and reactive (semiconductor) surfaces. *Chem Rev* 93:267–300
- Karakitsou KE, Verykios XE (1993) Effects of alervalent cation doping of titania on its performance as a photocatalyst for water cleavage. *J Phys Chem* 97:1184–1189
- Knopps-Gerrits PP, De Vos DE, Feijen EJP, Jacobs PA (1997) Raman spectroscopy on zeolites. *Microporous Mater* 8:3–17
- Kumar KNP (1995) Growth of rutile crystallites during the initial stage of anatase-to-rutile transformation in pure titania and in titania-alumina nanocomposites. *Scripta Metall Mater* 32:873–877

- Kumar K-NP, Keizer K, Burggraaf AJ, Okubo T, Nagamoto H, Morooka S (1992) Densification of nanostructured titania assisted by a phase transformation. *Nature* 358:48–51
- Lee GH, Zuo HM (2004) Growth and phase transformation of nanometer-sized titanium oxide powders produced by the precipitation method. *J Am Chem Soc* 87:473–479
- Li C (2003) Identifying the Highly Isolated Transition Metal Ions/Oxides in Molecular Sieves and on Oxide Supports by UV Resonance Raman Spectroscopy. *J Catal* 216:203–212
- Li C, Li MJ (2002) UV Raman spectroscopic study on the phase transformation of ZrO_2 , Y_2O_3 - ZrO_2 and SO_4^{2-}/ZrO_2 . *J Raman spectrosc* 33:301–308
- Li C, Stair PC (1996a) An advance in Raman studies of catalysts: ultraviolet resonance Raman Spectroscopy. *Stud Surf Sci Catal* 101:881–890
- Li C, Stair PC (1996b) Ultraviolet Raman spectroscopy characterization of sulfated zirconia catalysts; fresh, deactivated and regenerated. *Catal Lett* 36:119–123
- Li C, Stair PC (1997) Coke formation in zeolites studied by a new technique: ultraviolet resonance Raman spectroscopy. *Stud Surf Sci Catal* 105:599–606
- Li C, Xiong G, Xin Q, Liu JK, Ying PL, Feng ZC, Li J, Yang WB, Wang YZ, Wang GR, Liu XY, Lin M, Wang XQ, Min EZ (1999) UV resonance Raman spectroscopic identification of titanium atoms in the framework of TS-1 zeolite. *Angew Chem Int Ed* 38:2220–2222
- Li J, Xiong G, Feng ZC, Liu ZM, Xin Q, Li C (2000) Coke formation during the methanol conversion to olefins in zeolites by UV Raman spectroscopy. *Micro Meso Mater* 39:275–280
- Li MJ, Feng ZC, Xiong G, Ying PL, Xin Q, Li C (2001) Phase transformation in the surface region of zirconia detected by UV Raman spectroscopy. *J Phys Chem B* 105:8107–8111
- Li MJ, Feng ZC, Ying PL, Xin Q, Li C (2003) Phase transformation in the surface region of zirconia and doped zirconia detected by UV Raman spectroscopy. *Phys Chem Chem Phys* 5:5326–5332
- Linsebigler AL, Lu GQ, Yates JT Jr (1995) Photocatalysis on TiO_2 surfaces: principles, mechanisms, and selected results. *Chem Rev* 95:735–758
- Loddo V, Marci G, Martí C, Palmisano L, Rives V, Sclafani A (1999) Preparation and characterisation of TiO_2 (anatase) supported on TiO_2 (rutile) catalysts employed for 4-nitrophenol photodegradation in aqueous medium and comparison with TiO_2 (anatase) supported on Al_2O_3 . *Appl Catal B* 20:29–45
- Ma W, Lu Z, Zhang M (1998) Investigation of structural transformation in nanophase titanium dioxide by Raman spectroscopy. *Appl Phys A* 66:621–627
- Mackenzie KJD (1975) The calcinations of titania: the effect of additive on the anatase-rutile transformation. *Trans J Br Ceram* 74:29–34
- Muscat J, Swamy V, Harrison NM (2002) First-principles calculations of the phase stability of TiO_2 . *Phys Rev B* 65:224112-1–224112-15
- Navrotsky A, Kleppa OJ (1967) Enthalpy of the anatase-rutile transformation. *J Am Ceram Soc* 50:626–630
- O'Regan B, Graetzel M (1991) A low-cost, high-efficiency solar cell based on dye-sensitized colloidal TiO_2 films. *Nature* 353:737–740
- Ohsaka T, Izumi F, Fujiki Y (1978) Raman Spectrum of Anatase, TiO_2 . *J Raman Spectrosc* 7:321–324
- Okada K, Yamamoto N, Kameshima Y, Yasumori A (2001) Effect of silica additive on the anatase-to-rutile phase transition. *J Am Ceram Soc* 84:1591–1596
- Ovenstone J, Yanagisawa K (1999) Effect of hydrothermal treatment of amorphous titania on the phase change from anatase to rutile during calcinations. *Chem Mater* 11:2770–2774
- Ozaki S, Iida Y (1961) Grain growth and phase transformation of titanium oxide during calcination. *J Am Ceram Soc* 44:120–127
- Penn RL, Banfield JF (1999) Formation of rutile nuclei at anatase 112 twin interfaces and the phase transformation mechanism in nanocrystalline titania. *Am Mineral* 84:871–876
- Ranade MR, Navrotsky A, Zhang HZ, Banfield JF, Elder SH, Zaban A, Borse PH, Kulkarni SK, Doran GS, Whitfield HJ (2002) Energetics of nanocrystalline TiO_2 . *Proc Natl Acad Sci USA* 99(suppl 2):6476–6481

- Sakthivel S, Hidalgo MC, Bahnemann DW, Geissen S-U, Murugesan V, Vogelpohl A (2006) A fine route to tune the photocatalytic activity of TiO₂. *Appl Catal B* 63:31–40
- Shannon RD, Pask JA (1965) Kinetics of anatase-rutile transformation. *J Am Ceram Soc* 48:391–398
- Sreethawong T, Suzuki Y, Yoshikawa S (2005) Synthesis, characterization, and photocatalytic activity for hydrogen evolution of nanocrystalline mesoporous titania prepared by surfactant-assisted templating sol–gel process. *J Solid State Chem* 178:329–338
- Stair PC, Li C (1997) Ultraviolet Raman spectroscopy of catalysts and other solids. *J Vac Sci Technol A* 15:1679–1684
- Tsai S-J, Cheng S (1997) Effect of TiO₂ crystalline structure in photocatalytic degradation of phenolic contaminants. *Catal Today* 33:227–237
- Wang R, Hashimoto K, Fujishima A, Chikuni M, Kojima E, Kitamura A, Shimohigoshi M, Watanabe T (1997) Light-induced amphiphilic surfaces. *Nature* 388:431–432
- West AR (1984) Solid state chemistry and its applications. Wiley, New York, p 174
- Xie YC, Tang YQ (1990) Spontaneous Monolayer Dispersion of Oxides and Salts onto surfaces of Supports: Application to Heterogeneous Catalysis. *Adv Catal* 37:1–43
- Xiong G, Li C, Feng ZC, Ying PL, Xin Q, Liu J (1999) Surface coordination structure of molybdate with extremely low loading on gamma-alumina characterized by UV resonance Raman spectroscopy. *J Catal* 186:234–237
- Xiong G, Li C, Li HY, Xin Q, Feng ZC (2000a) Direct spectroscopic evidence for vanadium species in V-MCM-41 molecular sieve characterized by UV resonance Raman spectroscopy. *J Chem Soc Chem Commun* 677–678.
- Xiong G, Feng ZC, Li J, Yang H, Ying PL, Xin Q, Li C (2000b) UV resonance Raman spectroscopic studies on the genesis of highly dispersed surface molybdate species on γ -alumina. *J Phys Chem B* 104:3581–3588
- Yan MC, Chen F, Zhang JL, Anpo M (2005) Preparation of controllable crystalline titania and study on the photocatalytic properties. *J Phys Chem B* 109:8673–8678
- Yang J, Mei S, Ferreira JMF (2000) Hydrothermal synthesis of nanosized titania powders: Influence of peptization and peptizing agents on the crystalline phases and phase transitions. *J Am Ceram Soc* 83:1361–1368
- Yoshinaka M, Hirota K, Yamaguchi O (1997) Formation and sintering of TiO₂ (anatase) solid solution in the system TiO₂-SiO₂. *J Am Ceram Soc* 80:2749–2753
- Zhang HZ, Banfield JF (2000a) Phase transformation of nanocrystalline anatase-to-rutile via combined interface and surface nucleation. *J Mater Res* 15:437–448
- Zhang HZ, Banfield JF (2000b) Understanding polymorphic phase transformation behavior during growth of nanocrystalline aggregates: insights from TiO₂. *J Phys Chem B* 104:3481–3487
- Zhang F, Zheng Z, Ding X, Mao Y, Chen Z, Yang S, Liu X (1997) Highly oriented rutile-type TiO₂ films synthesized by ion beam enhanced deposition. *J Vac Sci Technol A* 15:1824–1827
- Zhang YH, Chan CK, Porter JF, Guo W (1998) Micro-Raman spectroscopic characterization of nanosized TiO₂ powders prepared by vapor hydrolysis. *J Mater Res* 13:2602–2609
- Zhang J, Li MJ, Feng ZC, Chen J, Li C (2006) UV Raman Spectroscopic Study on TiO₂. I. Phase Transformation at the Surface and in the Bulk. *J Phys Chem B* 110:927–935
- Zhang J, Xu Q, Feng ZC, Li MJ, Li C (2008) Importance of the relationship between surface phases and photocatalytic activity of TiO₂. *Angew Chem Int Ed* 47:1766–1769
- Zhu J, Zheng W, He B, Zhang J, Anpo M (2004) Characterization of Fe-TiO₂ photocatalysts synthesized by hydrothermal method and their photocatalytic reactivity for photodegradation of XRG dye diluted in water. *J Mol Catal A* 216:35–43